Comparative Study on Strain-Induced Crystallization Behaviours of Sulphur cross-linked Guayule Natural Rubber and Synthetic Isoprene Rubber

Guayule natural rubber · Synthetic isoprene rubber · Strain-induced crystallization · Non-rubber components

Strain-induced crystallization (SIC) behaviours of sulphur cross-linked guayule natural rubber (S-GR) and synthetic isoprene rubber (S-IR) were investigated using quick *in situ* simultaneous synchrotron time-resolved wide-angle X-ray diffraction/tensile measurement at SPring-8. Higher contents of oriented amorphous segments at low strain and crystallinity in S-GR were detected than in S-IR. This difference was ascribable to the presence of non-rubber components and higher *cis* content in S-GR than S-IR. Aggregates of non-rubber components may play a role in physically cross-linking polymer to accelerate the SIC in S-GR. S-GR and S-IR had comparable crystallite size and volume upon stretching, but the number of crystallites in the former was about twice than in the latter, particularly at large deformation.

Vergleichende Studie des Verhaltens der dehnungsinduzierten Kristallisation von schwefelvernetzten Guayule-Naturkautschuk und synthetischen Isoprenkautschuk

Guayule Naturkautschuk · Synthetischer Isoprenkautschuk · Dehnungsinduzierte Kristallisation · Nicht-Kautschukbestandteile

Es ist das Verhalten der dehnungsinduzierten Kristallisation (SIC) von schwefelvernetzten Guayule Naturkautschuk (S-GR) und synthetischem Isoprenkautschuk (S-IR) mit schneller „In Situ" simultaner Synchrotron-zeitaufgelöster Weitwinkel-Röntgen-Diffraktometrie/Zug-Messungen an einem SPring-8 untersucht worden. Es wurden höhere Anteile von orientierten amorphen Segmenten bei niedriger Belastung und Kristallinität im S-GR als in S-IR detektiert. Dieses wurde Nicht-Kautschukbestandteilen und einem höheren cis-Gehalt des S-GR im Vergleich zum S-IR zugeschrieben. Aggregate von Nicht-Kautschukbestandteilen mögen eine Rolle für die Beschleunigung der physikalischen Vernetzung in S-GR spielen.

Figures and Tables:
By a kind approval of the authors.

Introduction

Globally, almost all commercial natural rubber (NR) is collected from a single source, *Hevea brasiliensis*. *Hevea* NR is the most indispensable material for heavy-duty tires (typically tires for aircraft and trucks) and about 50,000 other products [1-3]. However, the use of a single species to generate the global NR supply strongly poses risk to the sustainability of modern society. In addition, *Hevea* NR which is cultured in rainy tropical regions, has recently experienced biosecurity in addition to biodiversity problems [1,2,4]. Lack of *Hevea* NR has long been recognized as potentially disastrous to the global rubber supply [2,4-6] Therefore, studies on other rubber yielding plants have been resumed [1,2,4-6]. Guayule (*Parthenium argentatum*) has long been known to produce NR [7-10], and is a very most promising species as a next-generation of NR source among a large number of NR yielding plants [1,2,11-13]. The most important property of *Hevea* NR is its self-reinforcement ability, namely as the strain-induced crystallization (SIC) behaviour. The versatility of *Hevea* NR in industrial applications is ascribable to its outstanding tensile properties and excellent crack growth resistance, which are primarily due to its SIC ability [2,14-21].

The SIC of guayule NR has been investigated: for example, uncross-linked guayule NR showed the lower degree of crystallinity than uncross-linked *Hevea* NR, but still provided the higher crystallinity degree than uncross-linked synthetic isoprene rubbers containing low or high *cis* content [22]. However, the crystallinity degree became higher in guayule NR than *Hevea* NR when both rubbers were subjected to peroxide cross-linking [23]. These results were obtained from a birefringence measurement of pre-stretched samples with a very long exposure time of light to the samples. Therefore, the SIC behaviours may have contained significant stress relaxation effects because of the lengthy, non-real time measurement during stretching. Recently, Ikeda *et al.* reported the SIC behaviours of sulphur cross-linked guayule, rubber dandelion (*Taraxacum koksaghyz*) and *Hevea* NRs by using quick time-resolved simultaneous synchrotron WAXD measurement during tensile deformation *in situ* [24]. The SIC behaviours of cross-linked dandelion NR was comparable to cross-linked *Hevea* NR. However, the cross-linked guayule NR showed a superior SIC upon high stretching to cross-linked *Hevea* and dandelion NRs. When these three samples were compared, the following differences on their SIC properties were observed: the cross-linked guayule NR had larger oriented amorphous components and larger crystallite sizes parallel to the stretching di-

Authors

Preeyanuch Junkong, Takumi Ohashi, Treethip Phakkeeree, Yuta Sakaki, Yuko Ikeda, Kyoto, Japan, Atitaya Tohsan, Bangkok, Thailand, Katrina Cornish, Wooster, OH, USA

Corresponding author:
Prof. Dr. Ikeda Yuko
Faculty of Molecular Chemistry and Engineering
Kyoto Institute of Technology
Matsugasaki, Sakyo
Kyoto 606-8585, Japan
E-Mail: yuko@kit.ac.jp

rection than the cross-linked *Hevea* and dandelion NRs. In addition, the crystallite volumes and orientation fluctuations of the crystallites were larger and lower in cross-linked guayule NR than in the others, respectively. It was speculated that the differences of SIC behaviours among these three samples were because of their macromolecular structures and the amount of non-rubber components. The unique SIC properties of cross-linked guayule NR as compared to cross-linked *Hevea* and dandelion NRs were concluded to be due to the lower non-rubber components particularly a lack of proteins leading the less branched physical network structure. Therefore, in this study, it inspired us to compare the SIC behaviour of sulphur cross-linked guayule NR to that of sulphur cross-linked synthetic isoprene rubber of about 98% *cis* content, which is composed of a linear molecular structure without any non-rubber components.

Experimental section

Materials

Solid guayule NR produce by drying guayule latex was obtained from The Ohio State University, Ohio Agricultural Research and Development Center (OARDC). The average molecular weight (M_w) of the gel free fractions of guayule NR was supposed to be > 1.0×10^6 g/mol as measured by one of the authors [10,11,25]. Additionally, a synthetic isoprene rubber (IR2200; M_w = *ca.* 1×10^6 g/mol) supplied from JSR Co. Guayule NR was subjected to conventional acetone extraction in order to remove resins [26, 27]. Synthetic isoprene rubber was also purified similarly to guayule NR. The details of raw materials and description of acetone extraction were explained in previous paper [24].

Preparation of rubber compounds and cross-linked samples

Cross-linking reagents

Elemental sulphur (powder, 150 mesh), stearic acid (LUNAC S-25), zinc oxide (ZnO, average diameter 0.29 μm) and *N*-cyclohexyl-2-benzothiazole sulfenamide (CBS, Sanceler CM-G) were commercial grades for rubber processing and used as received. They were purchased from Hosoi Chemical Industry Co., Ltd., Kao Co., Sakai Chemical Industry Co., Ltd., and Sanshin Chemical Industry Co., Ltd., respectively.

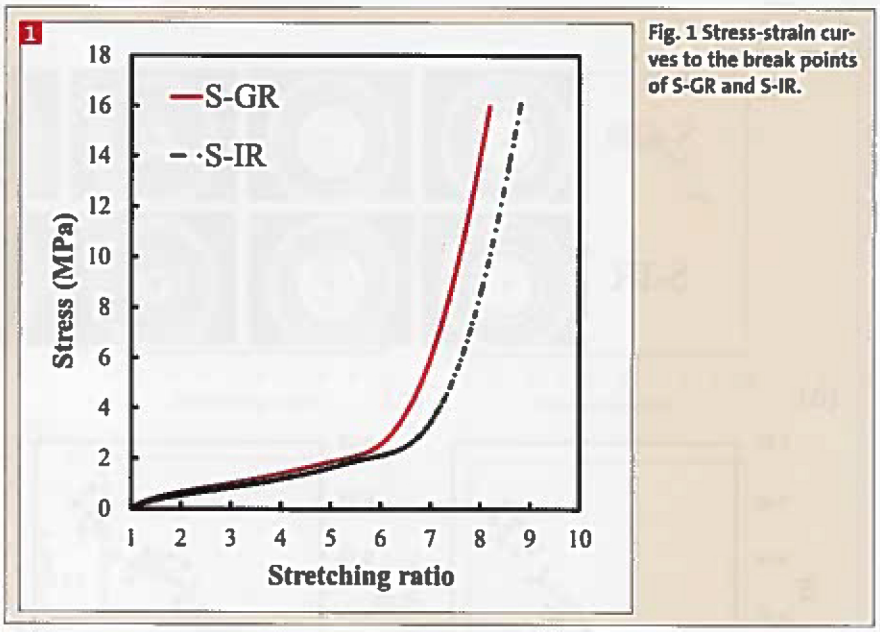

Fig. 1 Stress-strain curves to the break points of S-GR and S-IR.

Sample preparation

Each purified rubber was sulphur cross-linked (vulcanized). The rubber was mixed with ZnO of 1.0 parts per one hundred rubber by weight (phr), 2.0 phr stearic acid, 1.0 phr CBS and 1.5 phr sulphur using a conventional mixing on two-roll mill as described previously [24]. Here, the sulphur cross-linked samples were designated as S-GR and S-IR for guayule natural rubber and synthetic isoprene rubber, respectively. The raw (not vulcanized, but purified) rubbers are referred to as guayule NR and IR, respectively. The network-chain densities of the cross-linked rubbers were calculated by the modified Flory-Rehner equation [28] using the results of swelling test in toluene at 25°C [24] and shown in Table 1.

Simultaneous WAXD/tensile measurements

Synchrotron time-resolved wide-angle X-ray diffraction (WAXD) measurement was conducted during tensile deformation of the samples *in situ* at the BL-40XU beamline of SPring-8 in Harima, Japan. A custom-made tensile tester (ISUT-2201, Aiesu Giken, Kyoto) was set on the beamline and WAXD patterns were recorded during tensile measurement at room temperature. The wavelength of the X-ray was 0.08322 nm and the camera length was 131 mm. The two-dimensional WAXD patterns were recorded using a CCD camera (HAMAMATSU ORCA II). Intensity of the incident X-ray was attenuated using an aluminum plate equipped on the beamline. The sample was exposed to the incident beam for 70 ms every 3 s in order to minimize a relaxation effect in the SIC evaluation and radiation damage to the specimens during the measurement. The absorption correction for thinning of the samples under stretching was carried out using calculated correction coefficients, which were estimated on the basis of absorption coefficients per density [29,30] and weight fractions of each element in the samples. Ring-shaped samples were used in order to correctly measure the stretching ratio (α) of deformed samples. Inner and outer diameters of the ring-shaped specimens were 11.7 and 13.7 mm, respectively. Here, α is defined as $\alpha = l/l_0$, in which l_0 is the initial length and l

1 Characteristics of S-GR and S-IR

Sample code	Stress at α = 4.0 (MPa)	Stress at α = 5.5 (MPa)	Stress at α = 7.0 (MPa)	T_B[a] (MPa)	E_B[b]	Network-chain density[c] × 10^5 (mol/cm³)
S-GR	1.4	2.1	5.9	16.0	8.3	9.4
S-IR	1.2	1.9	3.4	16.2	8.8	8.6

[a] Tensile strength at break.
[b] Stretching ratio at break.
[c] Network-chain density determined by modified Flory-Rehner equation [28]

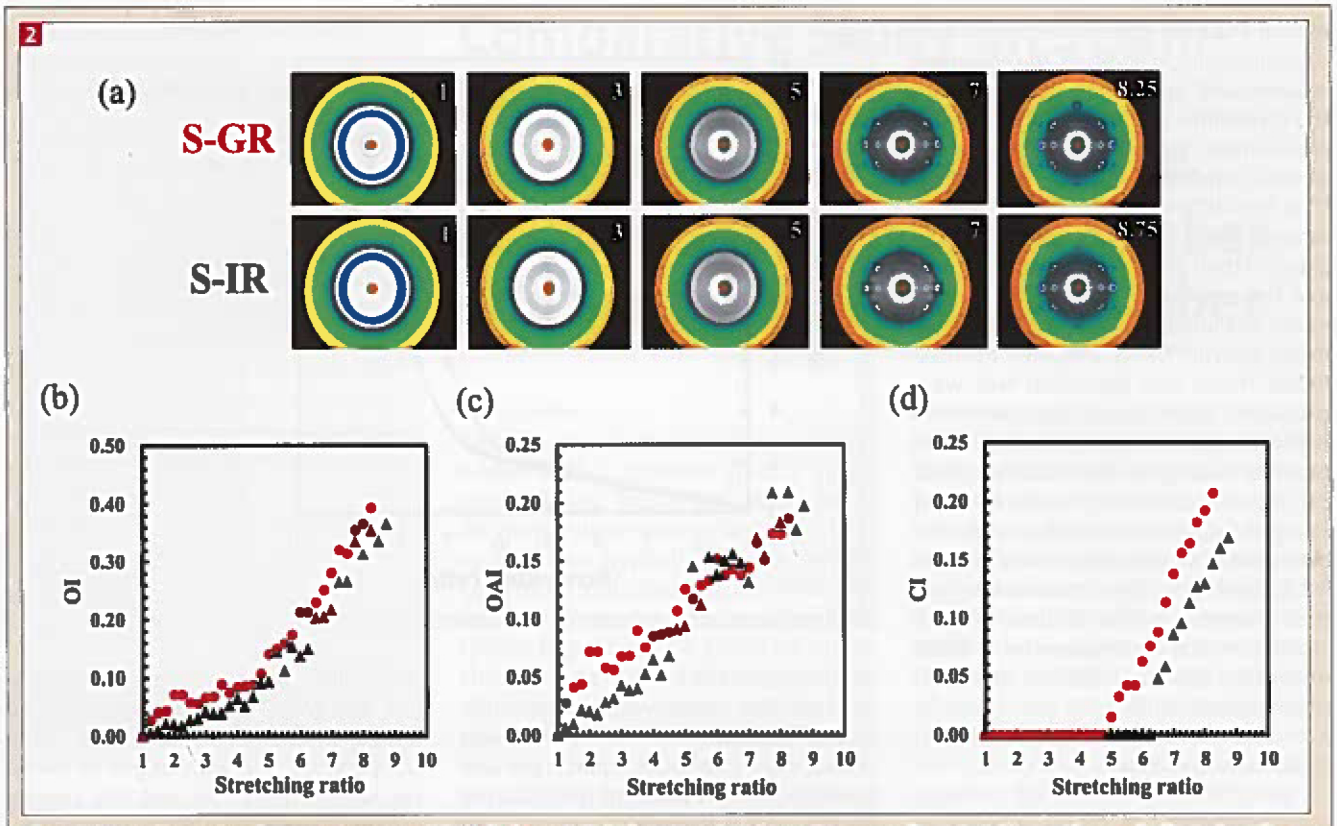

Fig. 2 (a) Two-dimensional WAXD patterns of S-GR (●) and S-IR (▲) during stretching. Corresponding stretching ratios are indicated on the right top of the images, and the variations of (b) OI, (c) OAI and (d) CI of S-GR and S-IR plotted against the stretching ratio.

is the length after deformation. The stretching speed was 100 mm/min, i.e., strain speed was about 4.98/min.

WAXD analysis

The obtained WAXD images were processed using "POLAR" (Stonybrook Technology & Applied Research, Inc.) [17,18]. The WAXD patterns of stretched samples were decomposed into three components, i.e., isotropic, oriented amorphous and crystalline components. The three components were azimuthally integrated within the range of ±75° from the equator. The details of this analytical method were described in our previous paper [17,18]. Three structural parameters, "crystallinity index (CI)", "oriented amorphous index (OAI)" and "oriented index (OI)", are calculated by the following equations, and "OI" is defined as OI = CI+OAI.

$$CI = \frac{\sum_{crystal} 2\pi \int \sin\phi d\phi \int I(s)s^2 ds}{\sum_{total} 2\pi \int \sin\phi d\phi \int I(s)s^2 ds} \quad (1)$$

$$OAI = \frac{\sum_{oriented-amorphous} 2\pi \int \sin\phi d\phi \int I(s)s^2 ds}{\sum_{total} 2\pi \int \sin\phi d\phi \int I(s)s^2 ds} \quad (2)$$

In eqn (1) and (2), $I(s)$ represents the intensity distribution of each peak that is read out from the WAXD pattern, s is the radial coordinate in reciprocal space in nm^{-1} unit ($s = 2(\sin\theta/\lambda)$, where λ is the wavelength and 2θ is the scattering angle), and ϕ is the angle between the scattering vector of the peak and the fiber direction.

Coherent lengths (apparent crystallite sizes) were estimated by using the Scherrer eqn (3) [31,32].

$$L_{hkl} = K\lambda/(\beta\cos\theta) \quad (4)$$

where L_{hkl} is the apparent crystallite size in the direction perpendicular to the (hkl) plane, and θ is the Bragg angle (half of the scattering angle). In this study, a value of 0.89 was used for K [32,33]. β was determined as follows: the intensity distribution on the equator was extracted from the original WAXD pattern, and each peak was fitted with a linear background and a Gaussian function having the form $I(x) = h \exp[-(x - x_c)^2/(2w^2)]$, where $I(x)$ is the intensity at position x, and x_c is the position at the scattering maximum. Parameters h and w are related to the peak height and peak width, respectively [17]. Each w value was converted into the half-width β.

Orientation fluctuation of 200 reflection was evaluated from the azimuthal scan of the peak [17]: the width parameter in the azimuthal direction (w_{az}) was obtained by fitting the intensity distribution with a Gaussian function. Then, w_{az} was converted into half-width β_{az} by the following equation:

$$\beta_{az} = 2w_{az}\sqrt{-2\ln(1/2)} \quad (5)$$

Moreover, it was reported that when an angle between the (120) and the (020) directions was nearly 19°, the value of L_{020} was approximated as $0.94L_{120}$ [34]. This observation agrees well with the angle estimated by the value of lattice constants in our experimental data. Ultimately, an average volume of crystallites (V_c) is defined as follows [34].

$$V_c = L_{200}L_{020}L_{002} = 0.94L_{200}L_{120}L_{002} \quad (6)$$

Assuming that crystallites have identical dimensions at a given stretching ratio, an average number of the crystallites per unit volume can be calculated using the V_c [34]. However, the CI value

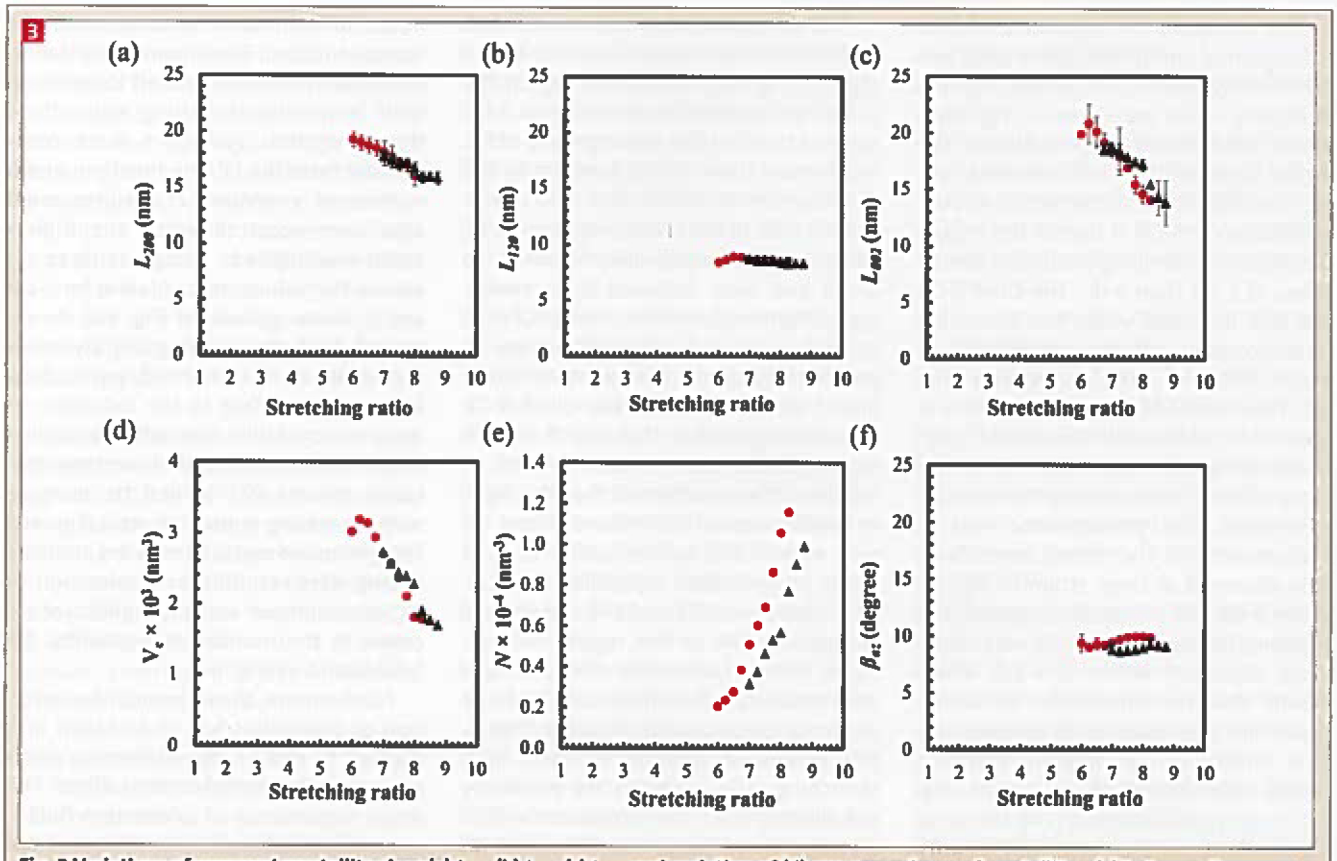

Fig. 3 Variations of apparent crystallite sizes (a) L_{200}, (b) L_{120}, (c) L_{002}, and variation of (d) average volume of crystallites, (e) indexes of average number of crystallites and (f) orientation fluctuation of crystallites for S-GR (●) and S-IR (▲) plotted against the stretching ratio.

in this study was the crystallinity index. Therefore, the index of average number of the crystallites per unit volume (N) was calculated as eqn (7)

$$N = \frac{CI}{V_c} \qquad (7)$$

Results and Discussion

1. Tensile properties and SIC behaviours of S-GR and S-IR

Fig. 1 shows the tensile stress-strain curves of sulphur cross-linked guayule natural rubber (S-GR) and sulphur cross-linked synthetic isoprene rubber (S-IR). The tensile stresses at α = 4, 5.5 and 7, tensile strengths at break (T_b) and the stretching ratios at break (E_b) of S-GR and S-IR with their network-chain densities are summarized in Table 1. It was clearly observed that the tensile stress-strain curves of S-GR and S-IR were different even though they were prepared using the same compound recipe. The tensile stress of S-GR was slightly higher than that of S-IR at low strain (α < 6), but the stress became significantly higher in S-GR than S-IR after the stress upturn at $\alpha \geq 6$. Notably, however, the slope of increasing stress at large strain was similar between S-GR and S-IR. The higher network-chain density of S-GR than S-IR as shown in Table 1 is likely the cause of the superior tensile stress of S-GR than S-IR. It should be kept in mind that the data obtained by swelling in toluene, which affects neither the physical nor the chemical cross-links, are related to a total „effective" cross-link density [35]. In addition, the non-rubber components in guayule NR are mostly hydrophilic and insoluble in toluene. Therefore, the higher network-chain density of S-GR may be contributed by not only the chemical cross-linking, but also physical interaction between non-rubber components and entanglement of rubber chains. In fact, the presence of non-rubber components, i.e., fatty acid/esters, but the absence of detectable proteins in purified guayule NR were confirmed by elemental analysis and Fourier-transform infrared spectroscopy as reported previously [24].

As shown above, the difference of network-chain density between these two samples does not much affect the tensile stress at α < 6. Only 20% increase of stress at low strain for S-GR was obtained. Therefore, the significantly larger tensile stress of S-GR than S-IR of approximately 70% after their stress up-turn points may be related not only to the network characteristics but also to the self-reinforcement effect caused by strain-induced crystallization (SIC) behaviours.

The 2D-WAXD patterns of S-GR and S-IR collected at α = 1, 3, 5, 7 and just before breaking point (α = 8.25 and 8.75 for S-GR and S-IR, respectively.) are displayed in Fig. 3a. The 2D-WAXD patterns between S-GR and S-IR were very similar at each stretching ratio. Before stretching at α = 1, an amorphous halo ring was observed in 2D-WAXD patterns of both S-GR and S-IR, indicating a presence of randomly coiled amorphous chains in the samples. Upon stretching, a crystalline reflection appeared together with the amorphous halo in the background in both samples. These phenomena are normal for *cis*-1,4-polyisoprene as reported in our previous articles [17-19]. However, the crystalline reflection intensities of S-GR were higher than S-IR at the large strain of α = 7. In order to clarify the SIC behaviours of both S-GR and S-IR, quantitative analysis was conducted.

The variations of the oriented index (OI), oriented amorphous index (OAI) and crystallinity index (CI) values against stretching ratios are shown in Fig. 3b, c and d, respectively. S-GR exhibited the higher OI than S-IR at all stretching ratios. This confirms that the better rubber orientation in S-GR is one of the important factors underlying the higher tensile stress of S-GR than S-IR. The OI of S-GR and S-IR increased when the stretching ratio increased with the maximum OI of about 39% and 37%, respectively (Fig. 3c). This means that the S-GR and S-IR both still contained unoriented segments of about 60%, even when the samples were stretched up to the rupture point. This phenomenon was in agreement with the strong amorphous halo observed at large strain in Fig. 3a. When S-GR and S-IR were compared, the suddenly increased OI of S-GR was recognized, especially before α = 2.5, which means that the orientation of rubber chains in S-GR can occur immediately after stretching. This feature was also clearly observed in the OAI results (Fig. 3c). In our previous report [24], the quite high molecular weight and high linearity of polyisoprene of guayule NR possibly contributed to the immediate orientation of chains upon stretching. If so, why was the sudden increase of OAI not observed in S-IR? This may relate to the presence of non-rubber components in guayule NR. As Ikeda et al. reported the presence of physically cross-linking network in *Hevea* NR [36], the non-rubber components such as fatty acids and esters in guayule NR may be physically aggregated in the polyisoprene rubber matrix. As a result, the aggregated parts may work as cross-linking sites, which accelerate the orientation of rubber chains in S-GR to the stretching direction. This consideration is supported by the earlier onset of SIC of S-GR than S-IR. While OAI of both S-GR and S-IR tended to increase with increasing stretching ratio, OAI of S-GR became similar to S-IR at $\alpha \geq 5.0$ and the onsets of SIC were found at α = 5 and 6.5 for S-GR and S-IR, respectively (Fig. 3d). Till now, the nucleating effect of fatty acids has been accepted as a factor, which accelerates SIC of NR, but this would have a trivial effect. The effect of the extended chains may be an important factor for the SIC progress [37]. Note that the guayule NR has better regularity of *cis*-1,4-microstructure than IR [37], which contributes to the SIC behaviour of S-GR.

The development of SIC in S-GR and S-IR was noticed to be separated into 2 regions (Fig. 3d): In the first region ($5 \leq \alpha \leq 6$), the physical cross-linking in S-GR seemed to affect the development of SIC much more than in S-IR. Specifically, the development of SIC in S-GR was slower than in S-IR. In the second region ($\alpha \geq 6$), some physical cross-links seemed to break and were followed by a similar crystallization speed (the slope of CI *vs* α) in both S-GR and S-IR, which may be governed by comparable chemical cross-linked structures. However, CI of S-GR was still higher than that of S-IR in both regions at the same stretching ratio. In addition, it was confirmed that the higher tensile stress of S-GR than S-IR at $\alpha \geq 6$ was mainly due to the ability of load stress by generated crystallites in S-GR. This is because S-GR and S-IR showed the comparable OAI in this region. Furthermore, the characteristics of strain-induced crystallites also influenced the large deformation behaviour of rubber. That is, the generated crystallites upon high stretching ratio acting as the physically crosslinking sites can accelerate and/or disturb the SIC behaviour. Thus, the SIC parameters for generated crystallites upon stretching are discussed in the next section.

2. The characteristics of strain-induced crystallites of S-GR and S-IR

Apparent crystallite sizes (coherent lengths) during stretching were determined from the WAXD profiles using the Scherrer equation. The calculated coherent lengths are reasonably assumed to reflect actual crystallite sizes. Fig. 4a, b and c show the variation of the apparent crystallite size estimated from the 200 (L_{200}), 120 (L_{120}) and 002 (L_{002}) reflections against strain, respectively, for S-GR and S-IR. At a specific stretching ratio, the difference of L_{200}, L_{120}, and L_{002} between S-GR and S-IR were not apparent. However, L_{002} of S-GR was slightly smaller than that of S-IR at high strain. As previously reported, the apparent crystallite sizes perpendicular to the (002) plane are assumed to relate to the length of fully stretched chains acting as the initiating species for SIC. It is speculated that the larger the L_{002}, the longer the fully stretched chains. Thus, the shorter fully stretched chains in S-GR than S-IR are attributable to the lower orientation of rubber chains to the stretching direction, which is due to the physical network structure of guayule NR with non-rubber components, as compared to linear synthetic isoprene rubber. The apparent crystallite size in all reflections tended to decrease with increasing stretching ratio. Thus, the generated crystallites were compressed from the lateral direction, and a rupture of generated crystallites must also have occurred when the higher strain was applied. Using the three L_{hkl} values, the volume of crystallite for S-GR and S-IR was calculated (Fig. 3d). As expected, S-GR showed very slightly lower crystallite volume than S-IR, particularly at large strain. Due to the reduction of apparent crystallite size with the applied stress for the samples, their average crystallite volume (V_c) tended to decrease with increasing stretching ratio (Fig. 4d). The generated crystallites acted as cross-linking sites resulting in acceleration of SIC development and the significant increase in the number of crystallites for S-GR than S-IR (Fig. 4e).

Furthermore, the influence of orientation of crystallites has to be taken into account to explain the reinforcing effect of the strain-generated crystallites. The strain dependence of orientation fluctuation of crystallites (β_{az}) for S-GR and S-IR are shown in Fig. 4f. Note that the obtained results were relative ones for the comparison between two samples. Here, small value of β_{az} means smaller fluctuations in orientation. Both samples have similar trends of the crystal fluctuation for the (200) plane: the crystal fluctuation abruptly decreased at the onset of SIC. Then, the crystal fluctuation became constant over increasing the stretching ratios. This may be due to compensation between the presence of strain-induced crystallites and the decrease in crystallite size. When considering a particular stretching ratio, the crystal fluctuation in S-GR was larger than that of S-IR. This difference may be attributed to the higher number of crystallite in S-GR and the disturbance of orientation of crystallites to the stretching direction by the larger non-rubber component in S-GR, when compared to S-IR.

Conclusion

This is the first report to reveal the characteristic differences of SIC behaviours between S-GR and S-IR, where the quick *in situ* simultaneous synchrotron time-resolved wide-angle X-ray diffraction/tensile measurement was conducted in the SPring-8. The results revealed a key function of non-rubber components in guayule NR as cross-linked sites as well as

the high regularity of *cis*-1,4-polyisoprene configuration of guayule NR to accelerate the SIC. The larger number of crystallites generated upon stretching in S-GR increased the stresses at high strains comparing with S-IR. It is also noted that the aggregated non-rubber components gave higher oriented amorphous segments at low strains in S-GR than in S-IR. These new results will be useful for rubber science and technology when guayule NR is utilized as a raw material to produce high performance NR products.

Acknowledgements

This work was supported by JST ALCA program (2015 -) to Y.I. The WAXD experiment was performed at the BL-40XU in the SPring-8 with the approval of the Japan Synchrotron Radiation Research Institute (JASRI) (Proposal Nos.2015A1872). We gratefully thank to Dr. S. Kohjiya, Professor Emeritus of Kyoto University, for his useful comments.

Notes and References

[1] S. Kohjiya, Smithers Rapra Publications, Shrewbury, (2015).

[2] Y. Ikeda, A. Tohsan, S. Kohjiya, ed. D. Reyes, Nova Science Publishers, New York, (2015), Chapter 3, pp. 35.

[3] Y. Hirata, H. Kondo, Y. Ozawa, *in Chemistry, Manufacturing and Applications of Natural rubber*, ed. S. Kohjiya, Y. Ikeda, Woodhead Publishing, Cambridge (2014), Chapter 12, pp. 325.

[4] M. J. W. Cock, M. Kenis, R. Wittenberg, Rubber Forestry Department, Food and Agricultural Organization (FAO) of the United Nations, Rome, (2003).

[5] R. Schultes, Bot. Rev. **36** (1970) 197.

[6] P. J. George, J. C. Kuruvilla, Rubber Research Institute of India, Kottayam (2000).

[7] F. E. Lloyd, Carnegie Institution of Washington, Washington D.C. (1911).

[8] W. W. Gordon, B.J. Stevenson, U. S. Department of Agriculture, Washington D. C. (1947).

[9] National Academy of Sciences, Books for Business, New York (2002). (Originally published in 1977.)

[10] J. B. van Beilen, Y. Poirier. Crit. Rev. Biotechnol. **27** (2007) 217.

[11] H. Mooibroek, K. Cornish, Appl. Microbiol. Biotechnol. **53** (2000) 355.

[12] M. R. Finlay, Rutgers University Press, New Brunswick (2009).

[13] K. Cornish, *in Chemistry, Manufacturing and Applications of Natural rubber*, S. Kohjiya, Y. Ikeda, Eds., Woodhead Publishing, Cambridge (2014), Chapter 1, pp. 3.

[14] A. H. Tullo, Chem. Eng. News., April 20 (2015) 18.

[15] S. Toki, I. Sics, S. Ran, L. Liu, B.S. Hsiao, S. Murakami, K. Senoo, S. Kohjiya, Macromolecules **35** (2002) 6578.

[16] S. Trabelsi, P. A. Albouy, J. Rault, Macromolecules **35** (2002) 10054.

[17] M. Tosaka, S. Murakami, S. Poompradub, S. Kohjiya, Y. Ikeda, S. Toki, I. Sics, B.S. Hsiao, Macromolecules **37** (2004) 3299.

[18] M. Tosaka, S. Kohjiya, S. Murakami, S. Poompradub, Y. Ikeda, S. Toki, I. Sics, B.S. Hsiao, Rubber Chem. Technol. **77** (2004) 711.

[19] Y. Ikeda, Y. Yasuda, K. Hijikata, M. Tosaka, S. Kohjiya, Macromolecules **41** (2008) 5876.

[20] Toki, *in Chemistry, Manufacturing and Applications of Natural rubber*, ed. S. Kohjiya, Y. Ikeda, Woodhead Publishing, Cambridge, (2014), Chapter 5, pp. 135.

[21] K. Bruning, Springer, Heidelberg (2014).

[22] Y. Shimimura, J.L. White, J.E. Spruiell, J. Appl. Polym. Sci. **27** (1982) 3553.

[23] I. S. Choi, Rubber. Chem. Technol. **70** (1997) 202.

[24] Y. Ikeda, P. Junkong, T. Ohashi, T. Phakkeeree, Y. Sakaki, A. Tohsan, S. Kohjiya and K. Cornish. RSC Advances. **6** (2016) 95601.

[25] P. Venkatachalam, N. Geetha, P. Sangeetha and A. Thulaseedharan. Afr. J. Biotechnol. **12** (2013) 1297.

[26] L. F. Ramos-De Valle, Rubber. Chem. Technol. **54** (1981) 24.

[27] C. McMahan, D. Kostyal, D. Lhamo, K. Cornish, J. Appl. Polym. Sci. **132** (2015) 2051(1).

[28] P.J. Flory, J. Chem. Phys. **18** (1950) 108.

[29] Y. Ikeda, Y. Yasuda, K. Hijikata, M. Tosaka, S. Kohjiya, Macromolecules **41** (2008) 5876.

[30] T. Hahn, in *International Tables for Crystallography*, D. Reidel Pub. Co., Holland, vol. A (1983) 157.

[31] P. Scherrer, Göttinger Nachrichten, **2** (1918) 98.

[32] H.P. Klug and L.E. Alexander, in *X-ray Diffraction Procedures for Polycrystalline and Amorphous Materials*, WileyInterscience, New York, 2nd edn (1974), pp. 687.

[33] S. Murakami, K. Senoo, S. Toki and S. Kohjiya, Polymer, **43** (2002) 2117.

[34] N. Candau, R. Laghmach, L. Chazeau, J. M. Chenal, C. Gauthier, T. Biben and E. Munch, Macromolecules, **47** (2014) 5815.

[35] E. Kontou, G. Spathis, M. Niaounakis, V. Kefalas. Colloid. Polym. Sci. **268** (1990) 636.

[36] T. Karino, Y. Ikeda, Y. Yasuda, S. Kohjiya and M. Shibayama. Biomacromolecules, **8** (2007) 693.

[37] S. Kohjiya, M. Tosaka, M. Furutani, Y. Ikeda, S. Toki and B. S. Hsiao. Polymer, **48** (2007) 3801.

SUPPLEMENT

Influence of Surface Roughness on Film Formation and Film Properties of Polypropylene Dipping Former

KGK 11-12/2016 Authors of the publication Influence of Surface Roughness on Film Formation and Film Properties of Polypropylene Dipping Former, KGK Kautschuk Gummi Kunststoffe, 69 (2016), p. 36 are Promsak Sa-Nguanthammarong, Bangkok, Thailand, Somboon Asavapichayachote, Pathumthani, Thailand, Krisda Suchiva, Supa Wirasate, Chakrit Sirisinha, Nakornpathom, Thailand; Corresponding author: Chakrit Sirisinha Rubber Technology Re search Centre, Faculty of Science Mahidol University, Salaya Campus, Nakornpathom, Thailand Tel: +662 441 9816 Ext. 1142 Fax: +662 441 0511 E-Mail: chakrit.sir@mahidol.ac.th.